

# The Impact of a Vortex Ring on Porous Surfaces—A Review

T.T. Lim and D. Adhikari

**Abstract** A vortex ring interacting with a solid surface have been studied extensively, both experimentally and numerically, for many years, however, there are relatively few studies made on the interaction with porous surfaces. Most of these studies were carried out recently and limited to laboratory investigations. This chapter provides an overview of the current state of knowledge on the interaction of a vortex ring on a porous surface and future research direction.

**Keywords** Vortex ring • Vortex ring/wall interaction • Porous surface

## 1 Introduction

A vortex ring or smoke ring refers to a bounded region of vorticity in a fluid where vortex lines form close loops. It comes in various shapes and sizes, and occurs naturally in situations such as rising of warm air or falling of cold air in atmosphere (for example, microburst), volcanic eruption, in the left ventricle of human heart during cardiac relaxation, nuclear explosion and insect flight to name just a few. Smokers sometimes produce them for amusement by blowing smoke through their mouth in a certain manner [7]. Also, cetaceans such as dolphins and beluga whales produce vortex ring bubbles occasionally for entertainment by puffing a burst of air through their blow hole in water [35, 37]. Vortex rings have fascinated scientists and engineers for more than 100 years (see Thomson [49]). The fascination is due partly to numerous engineering and biological applications, and partly to their compact

---

T.T. Lim (✉)

Department of Mechanical Engineering, National University of Singapore,  
Singapore, Singapore  
e-mail: mpelimmt@nus.edu.sg

D. Adhikari

School of Civil and Environmental Engineering, Georgia Institute of Technology,  
790 Atlantic Drive, Atlanta, GA 30332, USA

nature and profoundly interesting flow properties. Their compact nature make them ideal as a simpler building block in modelling more complex flows, such as turbulent free jets, hazardous downburst and propulsion of jelly fish and squids [16, 17]. On a more technological level, cavitating vortex rings, produced by exciting cavitating jets, have been used for underwater cleaning and rock cutting [10], and Akhmetov et al. [3] suggested using vortex rings for fighting oil well fires. Turner [51] and Fohl [22] proposed that vortex rings might be used to transport smoke or other effluents to higher atmosphere, thus reducing the necessity for tall chimneys. Numerous experimental, theoretical and numerical studies have been conducted on the generation, motion and interaction of vortex rings, and comprehensive reviews can be found in Shariff and Leonard [48], Lim and Nickels [33], and in a book by Saffman [47] and more recently by Akhmetov [2]. In this chapter, we focus primarily on the interaction of a vortex ring with a porous surface. The interaction has attracted considerable attention in recent years due partly to scientific interests and partly to its relevance in various complex flows such as static mixers and filters, flow transition to turbulence, etc.

There are various techniques of producing vortex ring in a laboratory, but the two most often used methods are by impulsively ejecting a slug of fluid through an orifice opening or a nozzle in quiescent fluid. The vortex generator can be a piston-cylinder arrangement [33] driven by a stepper motor (see Fig. 1) or by a pressurized

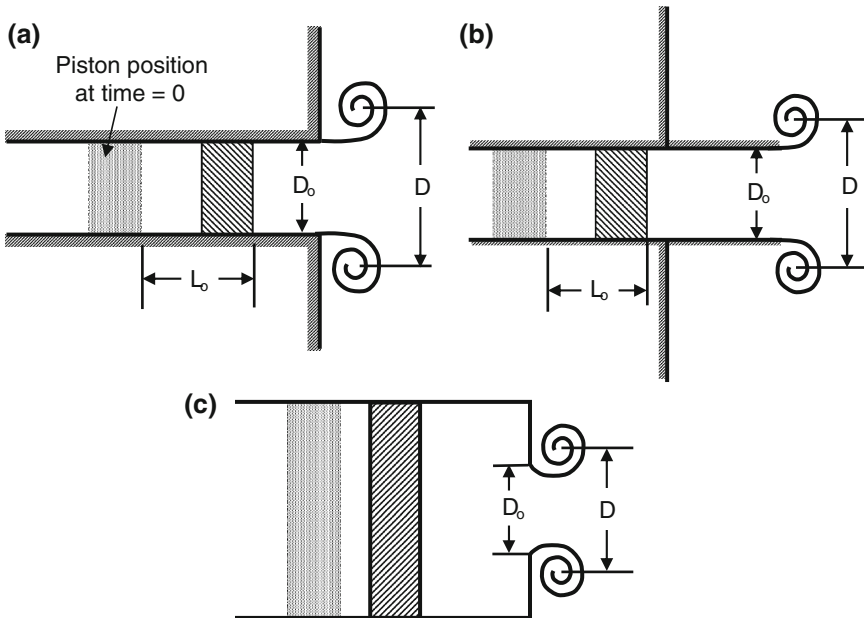


**Fig. 1** Schematics of some typical vortex ring generators using piston-cylinder arrangement. **a** Nozzle exit flushed with the side wall of a tank. **b** Nozzle exit protrudes into a tank. **c** Orifice opening

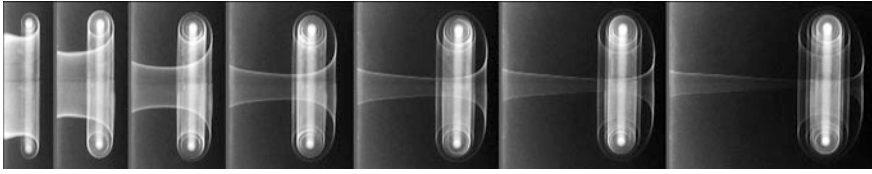


**Fig. 2** A vortex ring generated by nozzle type vortex ring generator. Here the roll up of a cylindrical shear layer into toroidal vortex can be clearly seen

air/water regulated vessel [41] or direct ejection of fluid using a vertical column of fluid [28]. The exit geometry of the orifice or nozzle (i.e. circular, elliptic or triangle, etc.) determines the shape, motion and stability of the resulting vortex ring [for example see 18, 29]. For a circular nozzle or orifice, the motion of the piston will cause a cylindrical vortex sheet to form at the edge of the nozzle or orifice before rolling up into a scroll as shown in Fig. 2. The fully developed vortex ring then propagates downstream through self-induced velocity.

In general, the diameter of a fully developed vortex ring ( $D$ ) is dependent on the ratio of stroke length ( $L_o$ ) and the nozzle diameter ( $D_o$ ). For a circular nozzle using the geometry shown in Fig. 1b, Auerbach [5] obtained the following empirical relations.

$$\frac{D}{D_o} = 1.18 \left( \frac{L_o}{D_o} \right)^{1/3} \quad \text{for } 0.3 \leq \frac{L_o}{D_o} \leq 1.0$$

$$\frac{D}{D_o} = 1.18 \left( \frac{L_o}{D_o} \right)^{1/5} \quad \text{for } 0.3 \leq \frac{L_o}{D_o} \leq 3.3$$

These expressions are restricted to  $1500 \leq Re_n \leq 4500$ , where  $Re_n$  is defined based on ejection velocity and nozzle diameter. In a subsequent experimental study by Gharib et al. [25] using a similar nozzle arrangement depicted in Fig. 1b, it is shown that a vortex ring cannot keep increasing in size with increasing  $L_o/D_o$ . They showed that the formation of an axisymmetric vortex ring is characterized by a time-scale that the vortex ring pinches off from its generating axisymmetric jet to form a well-defined vortex ring. Beyond this time-scale, larger vortex rings are not possible and the leading vortex ring is followed by a trailing jet. The transition between these two states occurs in a narrow range of stroke ratio ( $L_o/D_o$ ) between 3.6 and 4.5. They refer to this stroke ratio as “formation number”. At this formation number, the circulation that a vortex ring can acquire is at its maximum.

Once a vortex ring is fully developed, usually 1.5 nozzle diameter downstream [19], it propagates with a translation velocity that depends on the circulation ( $\Gamma$ ), vortex core radius ( $a$ ) and radius ( $R_o$ ) of the ring. For a thin core axisymmetric vortex ring, Saffman [44] derived an expression for the translation velocity ( $U$ ) given by

$$U \approx \frac{\Gamma}{4\pi R_o} \left\{ \log \left( \frac{4R_o}{\sqrt{\nu t}} \right) - 0.5880 \right\}$$

where  $\nu$  is the kinematic viscosity of fluid. The above expression is restricted to a very small time  $\left( \frac{\nu t}{R_o^2} \ll 1 \right)$  only. It also takes into account diffusing vortex core, which is assumed to have a Gaussian distribution of vorticity ( $\omega_\phi$ )

$$\omega_\phi = \frac{\Gamma}{4\pi \nu t} \exp^{-\frac{r^2}{4\nu t}}$$

where  $r$  is the core radius and  $t$  is time. In a more recent study, Fukumoto and Moffatt [23] extended the expression derived by Saffman [44] to a higher order using the variation principle and obtained the translation velocity as

$$U \approx \frac{\Gamma}{4\pi R_o} \left\{ \log \left( \frac{4R_o}{\sqrt{\nu t}} \right) - 0.5880 - 3.6716 \frac{\nu t}{R_o^2} \right\}$$

Past experimental studies have shown that if the Reynolds number (based on translation velocity and maximum ring diameter) is less than 600, a laminar vortex ring is formed. Once fully developed, the vortex ring propagates downstream with decreasing velocity while its volume increases with time. Reynolds [43] attributed the increased in volume to the entrainment of the surrounding fluid, which has the effect of causing the vortex ring to slow down in order to conserve momentum. However, Maxworthy [38] argued that the decrease in the propagation velocity may also be due to the shedding of vorticity in the wake. Under certain circumstances, a laminar vortex ring may undergo flow instability and develop azimuthal waves around its circumference. These instability waves grow with time and eventually transform a laminar vortex ring into a turbulent vortex ring, shedding vorticity in its wake as it propagates downstream. Detailed analysis of the azimuthal instability waves can be found in Widnall et al. [53], Tsai and Widnall [50], Widnall and Tsai [55] and Saffman [45] and the investigations on turbulent vortex rings can be found in Maxworthy [39], Glezer and Coles [26], Lim [32], and Gan and Nickels [24]. See also review articles by Shariff and Leonard [48] and Lim and Nickels [33].

In this chapter, we focus our attention only on the impact of a laminar vortex ring on porous surfaces. At the time of writing, the authors are not aware of similar studies where turbulent vortex rings are used. For completeness, we also include the case of a vortex ring interacting with a solid surface as this can be considered a special case of a porous surface with zero porosity. Besides, many of the flow features encountered during vortex ring/solid surface interaction are also observed during vortex ring/porous surface interaction.

## 2 Interaction of a Vortex Ring Normally with a Solid Surface

This particular interaction has been studied extensively both experimentally and numerically (for example, see [8, 9]; Walker et al. [14, 52]; Lim et al. [34, 42]; Doligalski et al. [20]; Chu et al. [15]; Fabris et al. [21]; Cheng et al. [13]). The interest is motivated partly by the fundamental physics involved and partly by its relevance in the study of turbulence wall bounded flow and in applications, such as flight of helicopters, turbulent flows in turbo-machines, geophysical flow, just to name a few.

An early experimental study of vortex ring/solid surface interaction was conducted by Magarvey and MacLachy [36]. Using smoke visualization technique, they observed the formation of a secondary vortex ring during the impact of a primary vortex ring on a plane surface. However, they erroneously attributed the formation of the secondary vortex ring to the uneven distortion of the vortex core of the primary vortex ring during the impact. In a similar experimental study using a vortex ring produced by impacting a drop of dyed water with the surface of the water, Boldes and Ferreri [8] observed the vortex ring rebounded from the solid surface, which they correctly attributed to the generation and separation of wall boundary layer. This finding is consistent with a related and earlier experimental study by Harvey and Perry [27], which show that boundary layer separation is responsible for the rebound of a pair of trailing vortices approaching the wall. Yamada et al. [56] arrived at the same conclusion from their experimental investigation using smoke visualization technique.

However, the most conclusive evidence showing that boundary layer separation and the subsequent generation of secondary vortex is responsible for the rebound of a primary vortex ring was provided by Lim et al. [34]. In their attempt to resolve the contentious issue of whether vortex rebound is caused by the generation and separation of wall boundary layer [8, 27] or the distortion of vortex core [6, 36], they performed two sets of experiments; one involved head-on collision of a vortex ring with a solid boundary and the other one involved head-on collision of two identical vortex rings. The latter experiment is equivalent to the interaction of a vortex ring with a “surface” in the absence boundary layer (i.e. free-slip condition). They argued that if vortex rebound is indeed caused by the distortion of vortex cores, then the phenomenon should be observed in both sets of experiments. However, their result did not show any evidence of vortex ring rebound during the head-on collision of two vortex rings, and this led them to conclude that boundary layer separation was indeed responsible for the vortex ring rebound.

The most comprehensive experimental investigation of the impact of a vortex ring on a solid surface was performed by Walker et al. [52] (see also [9]) for a range of Reynolds number (based on translation velocity and diameter of a fully developed vortex ring) from less than 250 to about 3000. Using dye visualization technique, they observed detailed flow features induced by a variety of laminar vortex. For a vortex ring with a low initial Reynolds number of less than

approximately 250, they found that the ring slowed down and expanded in diameter as it approached a solid surface. Due to low circulation of the primary vortex ring, the boundary layer generated underneath the vortex core was not sufficiently strong to roll up to form a secondary vortex ring. A schematic drawing of this scenario is shown in Fig. 3a. This behavior is in contrast to inviscid analysis that takes no account of the boundary layer process and predicts ever expanding vortex ring diameter. In the presence of no slip condition at the surface, the radial expansion of the primary vortex ring was eventually arrested by cancellation with vorticity of opposite sign at the surface. However, when the initial Reynolds number was increased to greater than 250, Walker et al. [52] found that the induced velocity of the primary vortex was strong enough to cause boundary layer to separate and roll up to form a secondary vortex ring of opposite circulation. The presence of the secondary vortex ring influences the trajectory of the primary vortex ring and vice versa. In fact, it can be deduced using the Biot-Savart law that the primary vortex ring, with its higher circulation, caused the secondary vortex ring to orbit around it and shrunk in diameter. At the same time, the induced velocity of the secondary vortex caused the primary vortex ring to rebound from the wall as can be seen in Figs. 3b and 4a. For Reynolds number less than 600, the rebound of the primary vortex ring is accompanied by a reduction in the radial expansion of the vortex core. But as the Reynolds number of the primary vortex ring is increased, the enhanced

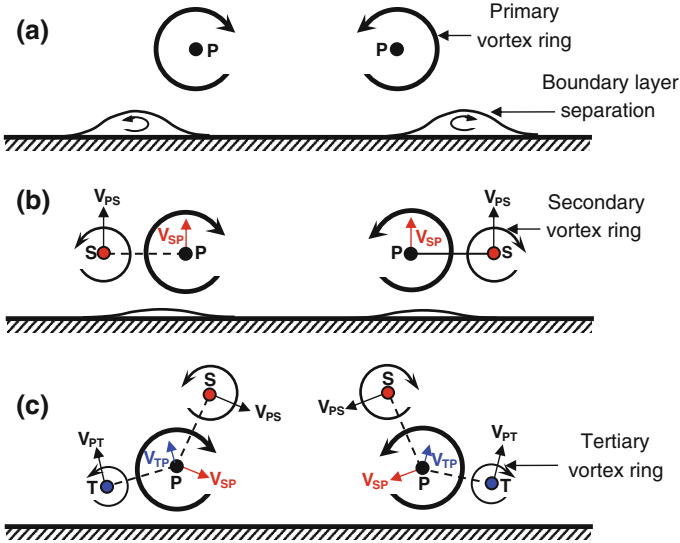


**Fig. 3** Schematic presentation of the interaction between primary vortex ring (P), secondary vortex ring (S) and tertiary vortex ring (T).  $V_{PS}$  and  $V_{PT}$  are the velocities induced by the primary vortex ring on the secondary and tertiary vortex rings, respectively.  $V_{SP}$  is the induced by the secondary vortex ring on the primary vortex ring, and  $V_{TP}$  is the induced by the tertiary vortex ring on the primary vortex ring. Note that the mutual induced velocities of the secondary and tertiary vortex rings are not shown to avoid complication

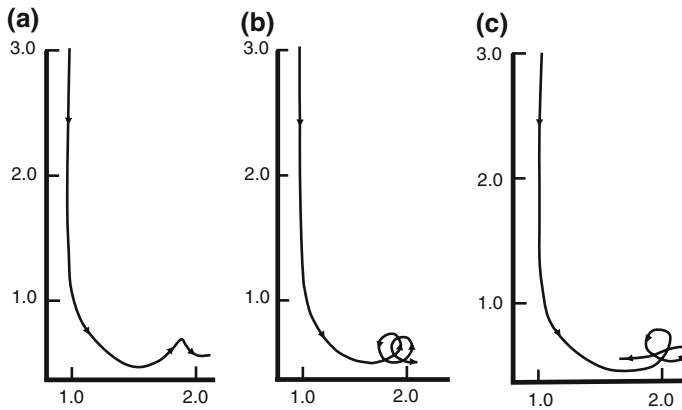


**Fig. 4** Trajectories of the right cores of the primary vortex rings based on the results of Walker et al. [52]. **a**  $Re = 564$ . **b**  $Re = 1680$ . **c**  $Re = 2550$

strength of the secondary vortex ring may be sufficiently strong to cause a momentary reversal in the radial velocity of the primary ring as can be seen in Fig. 4b. Similarly, a sufficient strong tertiary vortex ring can also cause the primary vortex ring to rebound. This is also reflected in Figs. 3c and 4b, where the first loop in the trajectory is due to the secondary vortex ring and the second loop is due to the tertiary vortex ring. For this particular case, despite the reversal in the core trajectory, the primary vortex ring, on the whole, continue to expand. However, at Reynolds number higher than  $Re = 2550$ , the trajectories can end up in permanent reversal as can be seen in Fig. 4c.

At low Reynolds number, the secondary vortex ring does not develop wavy instabilities during its interaction with the primary vortex ring, but at higher Reynolds number, secondary vortex ring can develop wavy instabilities that can affect the overall flow features. Walker et al. [52] attributed the instabilities of the secondary vortex ring to the compression of the secondary vortex filament as it orbits into the interior of the primary vortex ring, and not due to the azimuthal wavy instabilities often observed during the transition from a laminar vortex ring to a turbulent vortex ring as was discussed by Widnall and Sullivan [54]. The present wavy instabilities are found to induce an apparent waviness in the primary vortex ring, and the whole process eventually leads to degeneration into three dimensional chaotic ‘turbulent’ flow. These wavy instabilities occur in the Reynolds number range of 470–1600 only. At much higher Reynolds numbers, Walker et al. [52] observed another secondary vortex ring instabilities, which they termed as kink instabilities. Prior to the formation of the kink stability, the formation of the secondary vortex ring follows the same manner as that observed at lower Reynolds number. This kink instability does not appear to grow (in amplitude) once it orbits into the interior of the primary vortex ring and pauses for some time until the tertiary instability is formed and orbited around the primary vortex ring. This event triggers the ejection of the secondary vortex ring, and through its induced velocity

taking the tertiary vortex ring along with it. Due to the fact that the secondary and tertiary vortex rings possess circulation of the same sign, they eventually merge and propagate away from the surface.

Besides the experimental investigations, numerical simulations of the vortex ring/solid surface interaction have also been conducted by numerous researchers (for example, see Walker et al. [42, 52]; Chu et al. [15]; Fabris et al. [21]). The most recent study was performed by Cheng et al. [13], who used lattice Boltzmann method to compute the hydrodynamic behavior of a vortex ring during its interaction with a surface for a range of incidence angle ( $\theta$ ) from  $0^\circ$  to  $40^\circ$  and Reynolds number (based on translational velocity and initial diameter of the ring) from 100 to 1000. In this chapter, we restrict our discussion to the case of  $\theta = 0^\circ$ , in which the ring approaches the surface with its axis of symmetry normal to the surface. The salient feature of the flow, such as secondary and tertiary vortex rings are captured by the simulation and compare favorably with the experimental observation. In addition to the vortex structures, Cheng et al. [13] computed the dynamics of vortex stretching and surface pressure distribution during the interaction, which are difficult to obtain experimentally. Their results show that a vortex ring approaching a surface undergoes a slow rate of vortex stretching initially and a monotonic decrease in the rate of change of centre vorticity strength. As the vortex ring moves closer to the surface, the rate of radial expansion increases rapidly, and this is accompanied by a reduction in core size and vorticity intensification. This process enhances viscous diffusion and vorticity cancellation with the vorticity of opposite sign from boundary layer. As expected, higher Reynolds number produces higher rate of radial expansion, higher adverse surface pressure gradient and higher maximum stagnation pressure. These computed results provide valuable insight into the evolution of pressure and vorticity field during the impact.

### 3 Interaction of a Vortex Ring Normally with a Porous Surface

As far as the authors are aware, one of the earliest observations of vortex ring/porous surface interaction was recorded by Morton in his unpublished work (see Adhikari and Lim [1]). Morton commented that when “*the plane wall is replaced by a fine gauze (such as a fly screen), the motion of the ring is little affected at low Reynolds numbers but at higher Reynolds numbers the ring passes through the screen and continues as a modified vortex ring in its lee*”. Compared to vortex ring interacting with a solid surface, there are fewer studies on the interaction with porous surfaces. Most of them are conducted relatively recently via experimental investigation (see [1, 28, 41]). These studies show that although vortex ring/porous surface interaction shares many of the salient flow features found in vortex ring/solid surface interaction, the final outcomes of the interaction is very much dependent on screen porosity, wire diameter and Reynolds number of the



approaching primary vortex ring. The dependency on the Reynolds number and screen porosity for a fixed wire diameter was investigated by Adhikari and Lim [1] for screen porosity of 62 and 81 % and Reynolds number of a primary vortex ring from 384 to 2369. Their results of the vortex core trajectories versus non-dimensional time are presented in Fig. 5. Adhikari and Lim [1] categorized the interaction into four broad scenarios based on the transmitted flow through the screen. We now discuss each of these scenarios with reference to 62 % porosity screen.

Scenario 1 occurs when a low Reynolds number primary vortex ring impacts normally on a low porosity screen. One such example is presented in Figs. 5a and 6 for the case of  $Re = 384$  and  $\beta = 62\%$ , where the core trajectory and snapshots during the interaction are depicted. It can be seen from Fig. 5a that the trajectory of the vortex core interacting with the porous screen follows closely that of the corresponding interaction with a solid surface except near the end of the interaction where the two trajectories deviate. The deviation arises from the fact that the porous screen allows the self-induced velocity of the primary vortex ring to pass through it

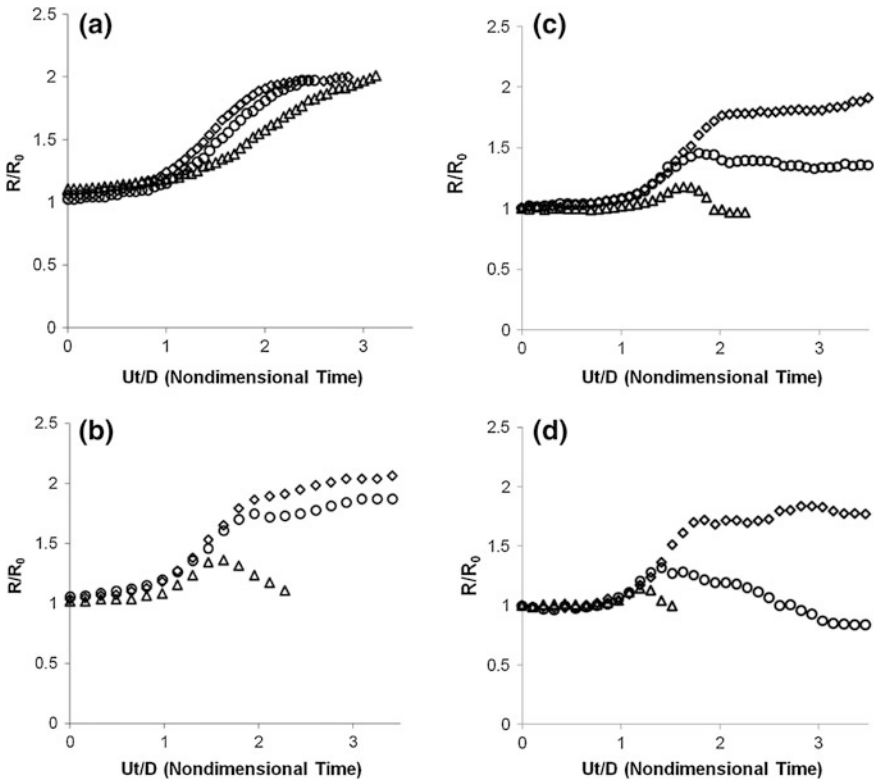


**Fig. 5** Radial expansion of the primary vortex ring versus non-dimensional time ( $t^* = Ut/D$ ) on a solid wall and porous screens. *Diamond* Solid Wall; *circle* 62 % Porosity; *triangle* 81 % Porosity. **a**  $Re_T = 384$ . **b**  $Re_T = 779$ . **c**  $Re_T = 1597$ . **d**  $Re_T = 2369$ . Reproduced from Adhikari and Lim [1]

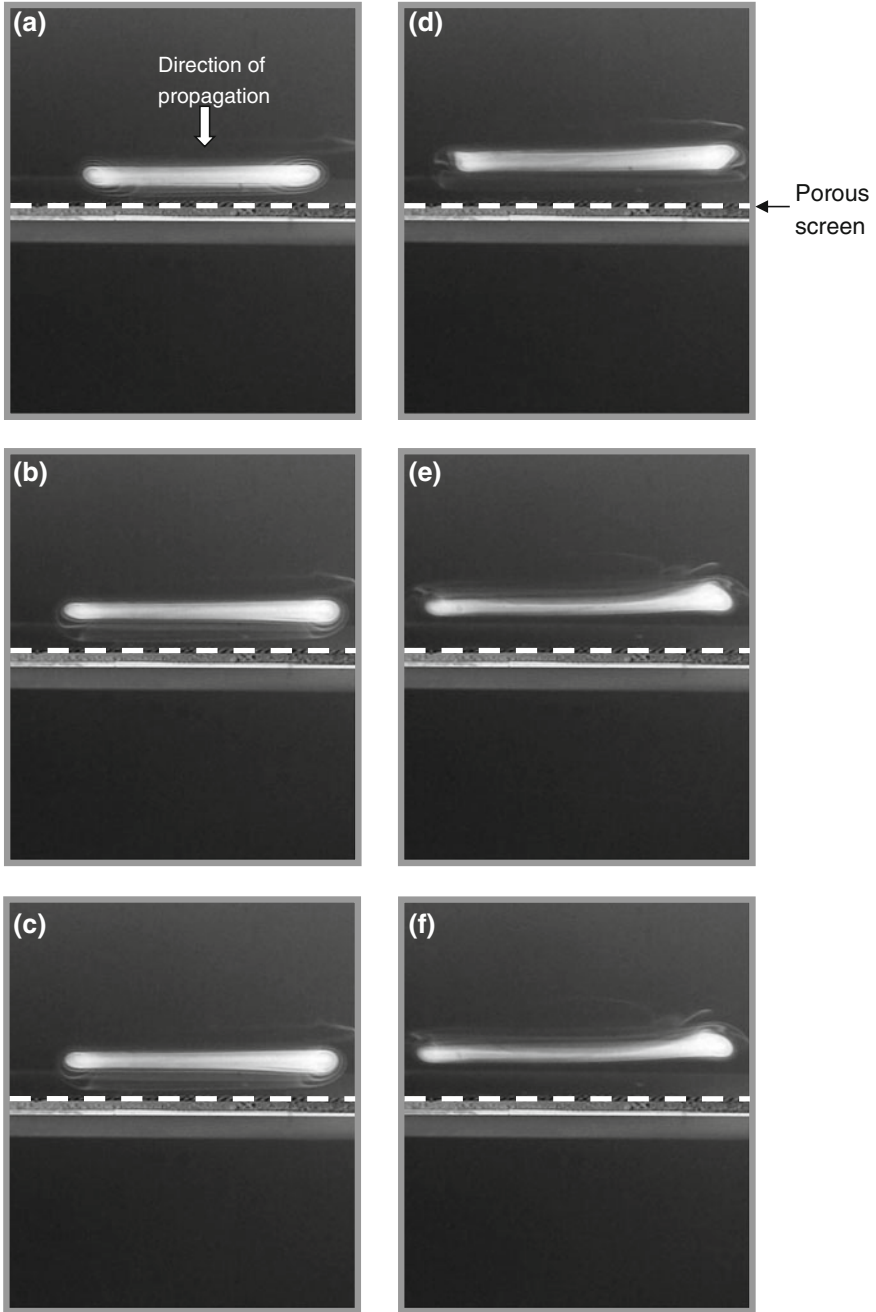
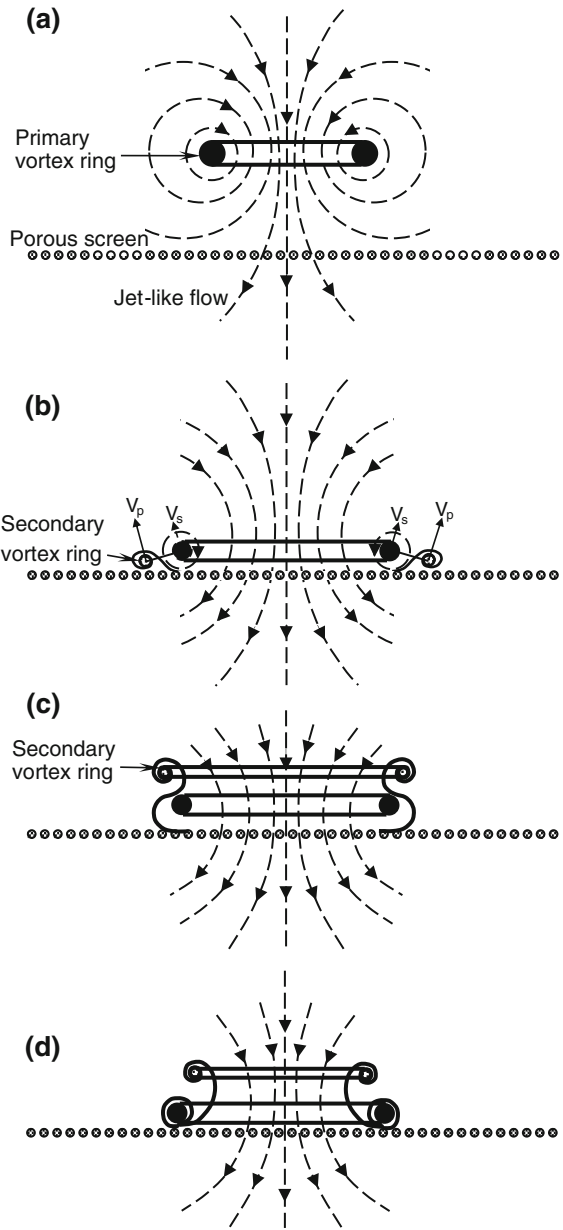


**Fig. 6** Impact of a vortex ring on a 62 % porosity screen for  $Re_T = 384$ . Time increases from (a) to (f).  $t^* = 0.0$  corresponds to the instance when the vortex ring is one ring diameter from the screen. Reproduced from Adhikari and Lim [1]. **a**  $t^* = 2.21$ . **b**  $t^* = 2.72$ . **c**  $t^* = 2.83$ . **d**  $t^* = 3.86$ . **e**  $t^* = 6.07$ . **f**  $t^* = 6.75$

to form a jet-like flow. Adhikari and Lim [1] referred to this kind of interaction, which produces the jet-like flow on the leeside of the screen as Scenario 1. Their interpretation of the interaction is illustrated in Fig. 7. This transmitted jet carried with it some of the original vorticity leaving behind a much weaker primary vortex

**Fig. 7** Adhikari and Lim [1]’s interpretation of the vortex ring/porous screen interaction at  $Re_T = 384$  (Scenario 1). Time increases from (a) to (d). Note that broken lines merely represent conceptual streamlines depicting the transmission of the induced flow of the toroidal ring through the screen. The actual streamline pattern is more complex. *Single arrows* represent direction of flow field. Reproduced from Adhikari and Lim [1]



ring to interact with the screen. As a consequent, a much weaker secondary vortex ring is generated resulting in a much weaker vortex rebound compared to a solid surface. The fact that the fluid passes through the screen suggests that the “symmetry plane” is broken and the method of images can no longer be applied generally throughout the whole flow field to explain the observed behavior. However, it can still be used as an approximation locally to explain the initial radial expansion of the primary vortex ring as it interacts with the screen.

When the Reynolds number of the primary vortex ring is increased to 779, the evolution of the primary vortex ring during the initial stages of the interaction with a porous screen still closely follow that of the interaction with a solid surface. Significant differences between these two surfaces emerged only near the end of the interaction as can be seen in Fig. 5b, which depicts the vortex core trajectory and in Fig. 8, which shows the corresponding flow visualization images during the interaction. Although not as clearly visible in Fig. 8, Adhikari and Lim [1] observed during the experiment that the transmitted jet for this case is now sufficiently strong, in terms of circulation, to roll up into a ring-like structure. This ring-like structure has circulation of the same sign as the primary vortex ring. Due to the presence of the porous screen, its influence on the trajectory of the primary vortex ring is limited compared to the influence of the secondary vortex ring. This interaction is schematically illustrated in Fig. 9 and Adhikari and Lim [1] referred to it as Scenario 2. The difference between Scenario 1 and 2 lies in the transformation of jet-like flow to ring-like structure.

Scenario 3 occurs at a much higher Reynolds number, where the ring-like structure developed into fully formed vortex ring. This can be clearly observed in Figs. 10 and 11 for cases of  $Re_\Gamma = 1597$  and 2369, respectively. Adhikari and Lim [1] referred to the newly formed ring as “regenerated vortex ring”. As in the previous cases, the porous screen limits the influence of the regenerated vortex ring on the trajectory of the primary vortex ring, but the close proximity of the secondary vortex ring to the primary vortex ring leads to their mutual interaction, which causes primary vortex ring to rebound from the screen and contract. At the same time, the primary vortex core, through its induced velocity, causes the secondary vortex core to orbit around it and towards the inner region of the primary vortex ring. At some stage, the self-induced velocity of the secondary vortex ring is able to escape the induced velocity field of the primary vortex ring and travels away from the screen. This process is similar to vortex ring/solid surface interaction and is clearly illustrated in Fig. 12.

Scenario 4 occurs at even higher Reynolds number and screen porosity. An example of which is shown in Fig. 13. Here, the primary vortex ring, after losing some of the vorticity to the regenerated vortex ring, is still sufficiently energetic to pass through the screen, leaving behind the secondary vortex ring on the approaching side of the screen. The modified “transmitted” primary vortex ring eventually pairs up with the regenerated vortex ring, and propagates as a whole away from the screen. This sequence of event is schematically presented in Fig. 14.

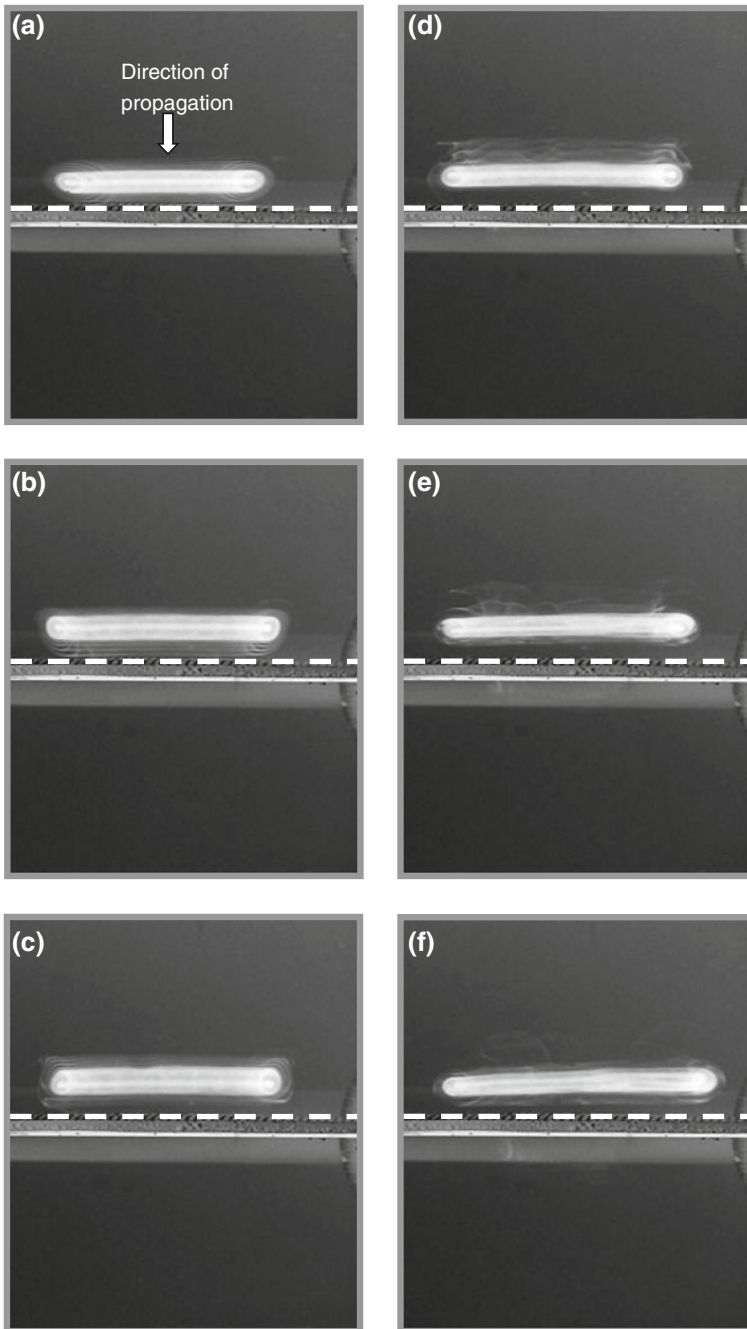
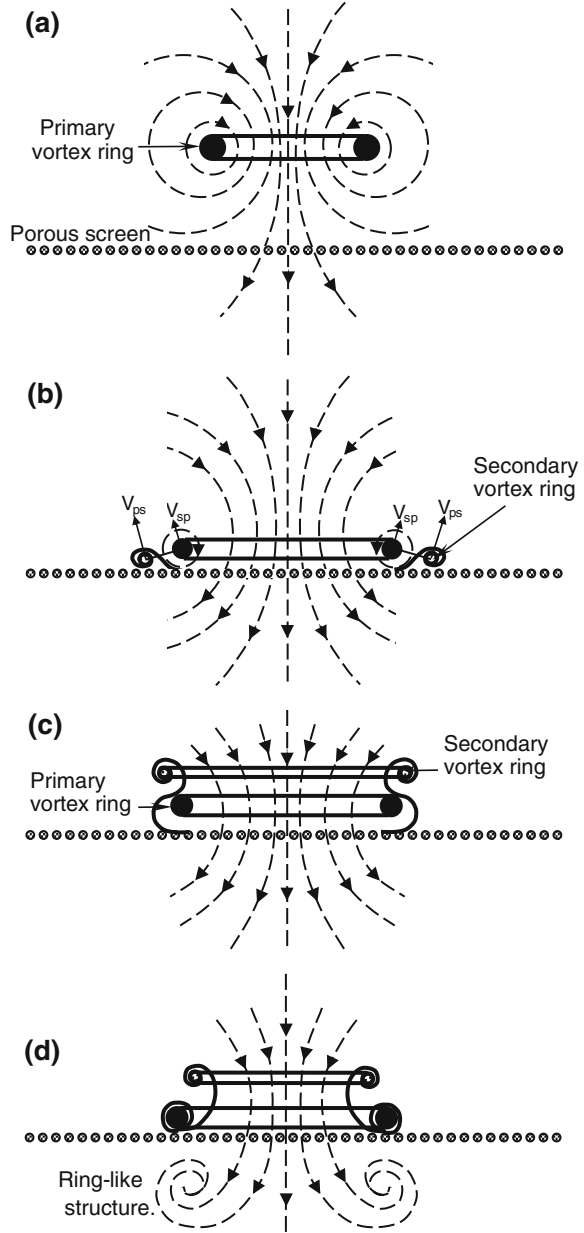
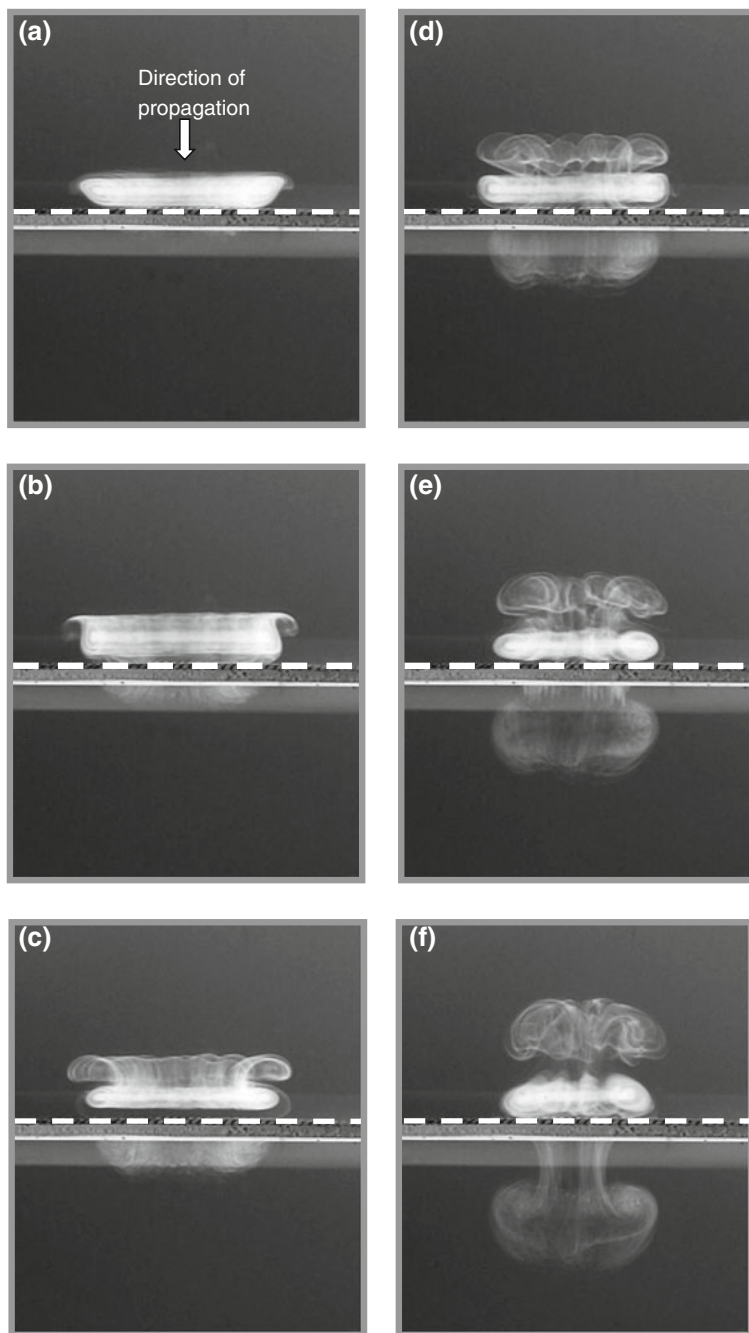


**Fig. 8** Impact of a vortex ring on a 62 % porosity screen for  $Re_T = 779$ . Time increases from (a) to (f).  $t^* = 0.0$  corresponds to the instance when the vortex ring is one ring diameter from the screen. Reproduced from Adhikari and Lim [1]. **a**  $t^* = 1.55$ . **b**  $t^* = 1.97$ . **c**  $t^* = 2.44$ . **d**  $t^* = 2.93$ . **e**  $t^* = 4.07$ . **f**  $t^* = 6.59$

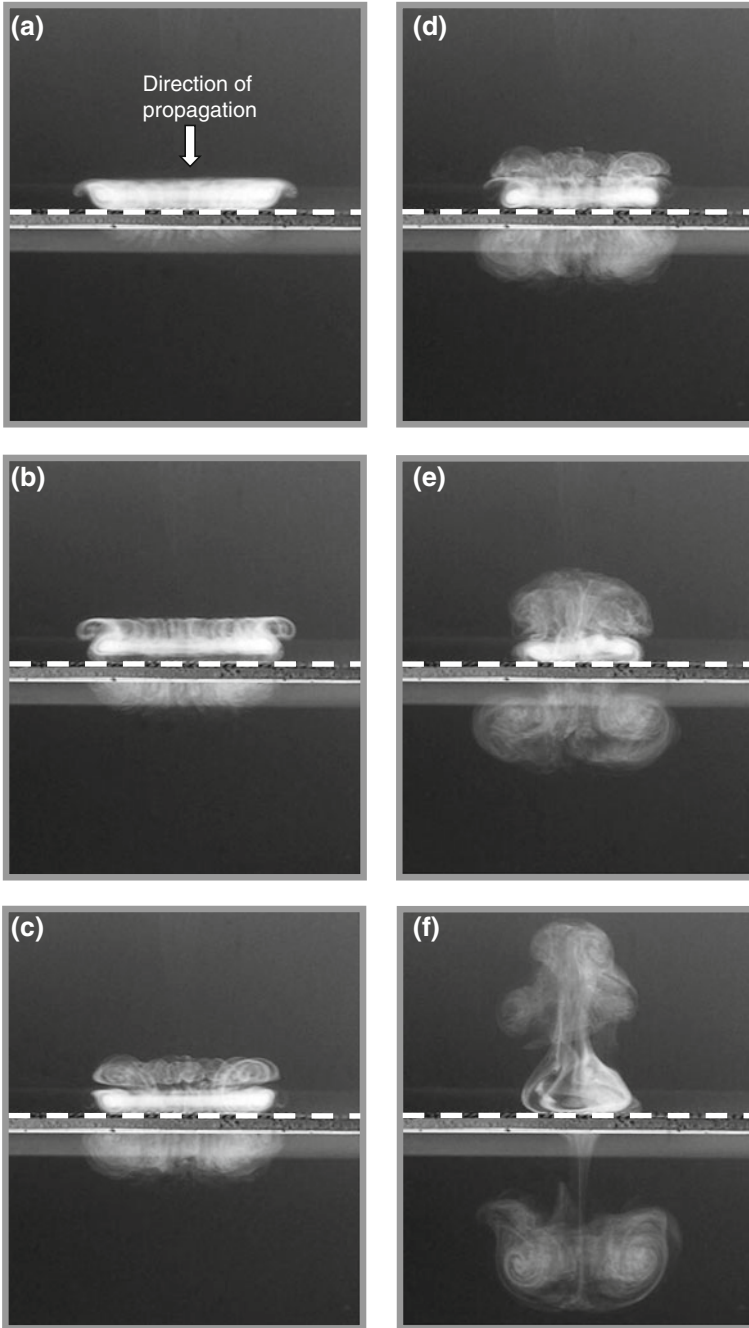
**Fig. 9** Adhikari and Lim [1]'s interpretation of the vortex ring/porous screen interaction at  $Re_F = 779$  (Scenario 2). Time increases from (a) to (d).  $V_{ps}$  = induced velocity of the primary vortex ring on the secondary vortex ring,  $V_{sp}$  = induced velocity of the secondary vortex ring on the primary vortex ring. Single arrows represent direction of flow field. Reproduced from Adhikari and Lim [1]



Adhikari and Lim [1] attributed the passage of the primary vortex ring through the screen to the mechanism of vortex stretching and reconnection (see also [4, 11, 30, 31, 40, 46]), and proposed a simplified model to explain it. When the Reynolds number is increased further, the interaction follows the same sequence of event as



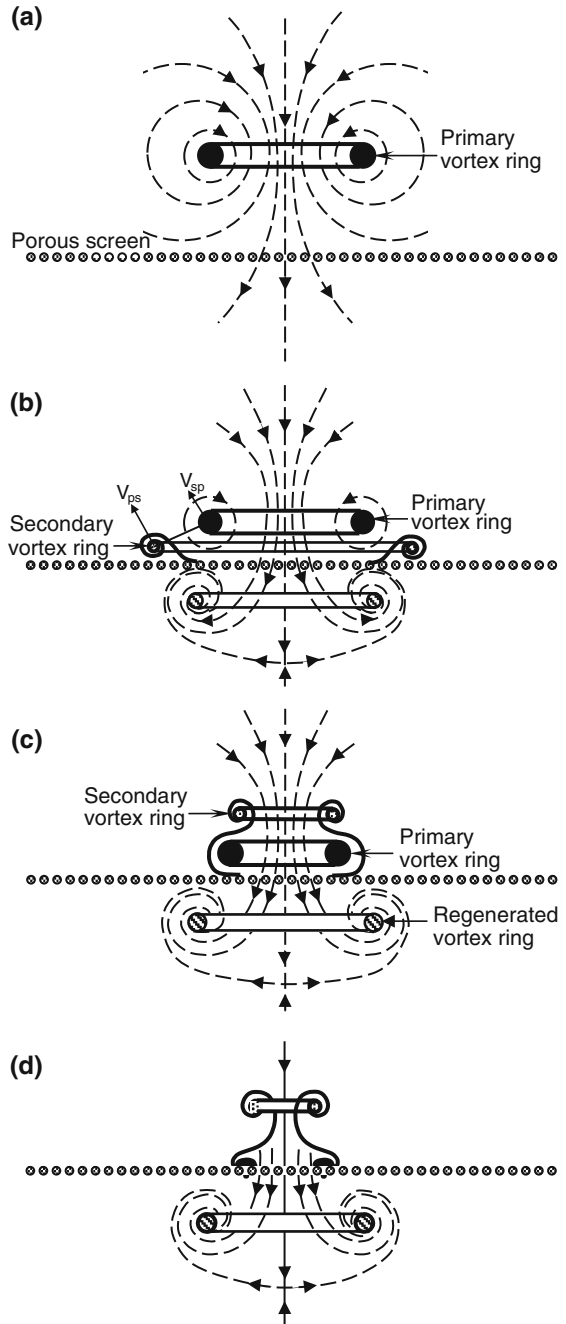
**Fig. 10** Impact of a vortex ring on a 62 % porosity screen for  $Re_T = 1597$ . Time increases from (a) to (f).  $t^* = 0.0$  corresponds to the instance when the vortex ring is one ring diameter away from the wall. Reproduced from Adhikari and Lim [1]. **a**  $t^* = 1.47$ . **b**  $t^* = 1.84$ . **c**  $t^* = 2.45$ . **d**  $t^* = 3.65$ . **e**  $t^* = 5.73$ . **f**  $t^* = 9.11$



**Fig. 11** Impact of a vortex ring on a 62 % porosity screen for  $Re_T = 2369$ . Time increases from (a) to (f).  $t^* = 0.0$  corresponds to the instance when the vortex ring is one ring diameter away from the wall. Reproduced from Adhikari and Lim [1]. **a**  $t^* = 1.19$ . **b**  $t^* = 1.57$ . **c**  $t^* = 2.14$ . **d**  $t^* = 2.56$ . **e**  $t^* = 4.16$ . **f**  $t^* = 9.49$



**Fig. 12** Adhikari and Lim [1] 's interpretation of Figs. 12 and 13 (Scenario 3). Time increases from (a) to (d).  $V_{ps}$  = induced velocity of the primary vortex ring on the secondary vortex ring,  $V_{sp}$  = induced velocity of the secondary vortex ring on the primary vortex ring. Only the induced velocity vectors on the left hand side of the vortices are shown in (b). *Single arrows* represent direction of flow field. Reproduced from Adhikari and Lim [1]



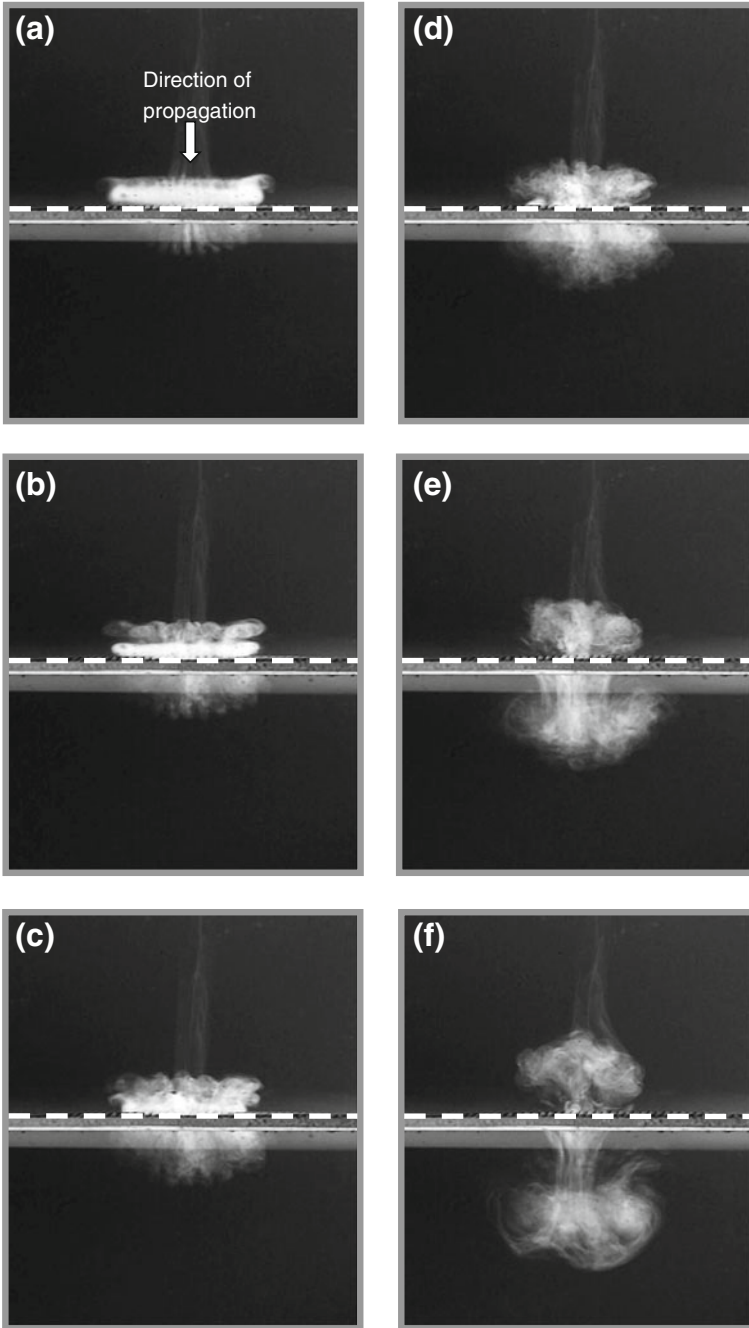
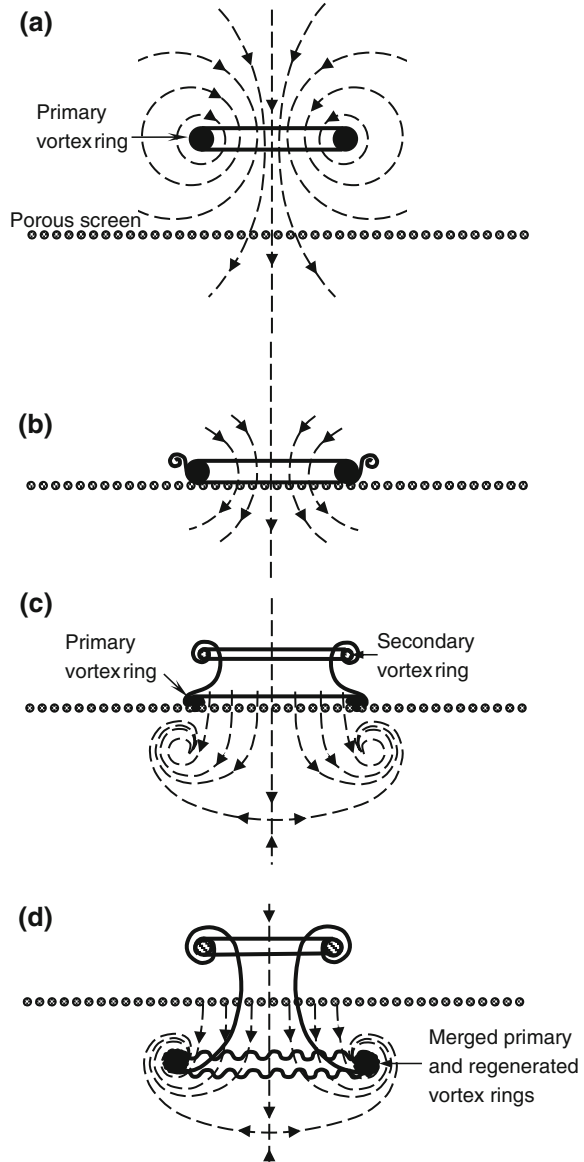


**Fig. 13** Impact of a vortex ring on a 62 % porosity screen for  $Re_T = 4026$ . Time increases from (a) to (f).  $t^* = 0.0$  corresponds to the instance when the vortex ring is one ring diameter away from the wall. Reproduced from Adhikari and Lim [1]. **a**  $t^* = 1.13$ . **b**  $t^* = 1.28$ . **c**  $t^* = 1.45$ . **d**  $t^* = 1.77$ . **e**  $t^* = 2.44$ . **f**  $t^* = 3.67$

**Fig. 14** Adhikari and Lim [1] 's interpretation of Fig. 15 (Scenario 4). Time increases from (a) to (d). The passage of the primary vortex ring through the screen is via a possible mechanism of vortex stretching and reconnection as detailed in Fig. 17. Note that the wavy ring in (d) is only a conceptual representation and the bridges as indicated in Fig. 17 are not shown here to avoid complication to the figure. *Single arrows* represent direction of flow field. Reproduced from Adhikari and Lim [1]



that in scenario 4, except that higher Reynolds number vortex ring is able to pass through the screen quicker and emerges on the leeside of the screen as a modified ring.

For higher porosity screen, Adhikari and Lim [1] found that the same four scenarios exist except that each scenario occurs at lower Reynolds number (see for example Fig. 15).

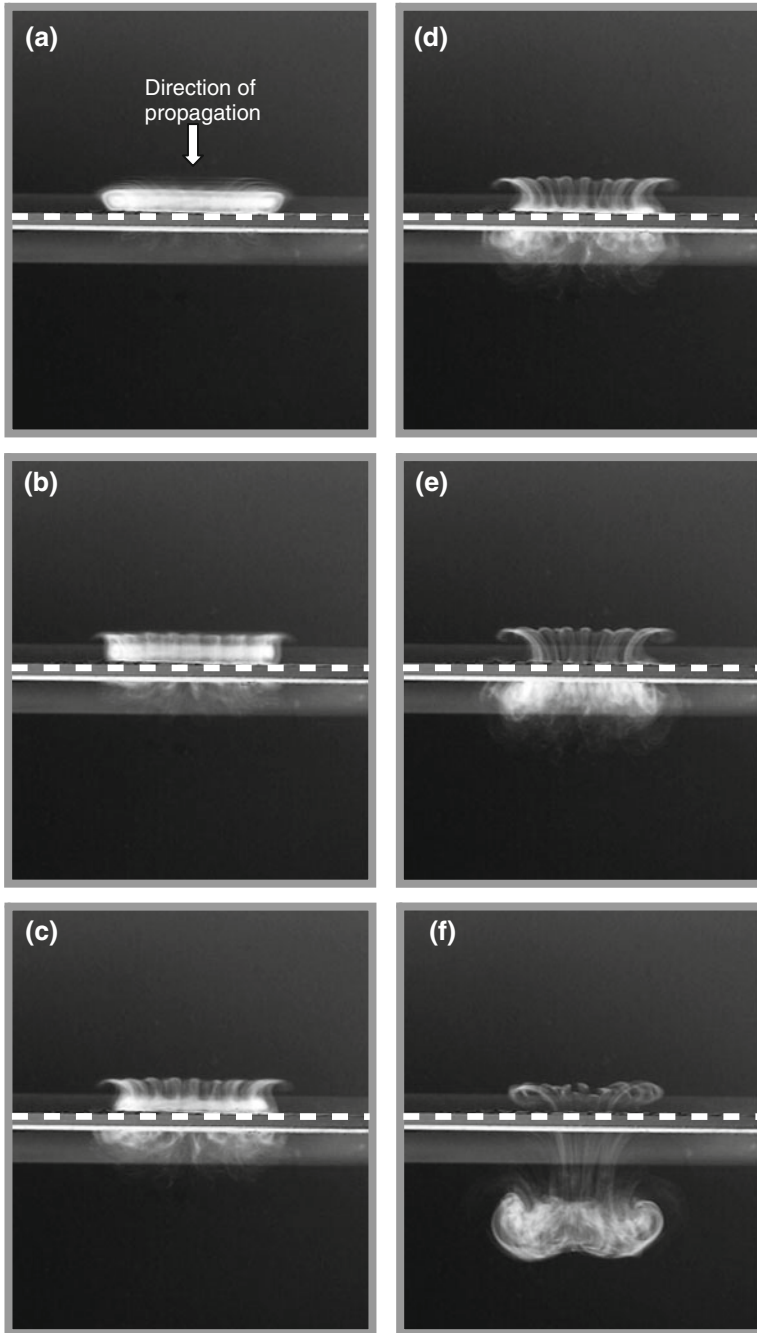


**Fig. 15** Impact of a vortex ring on a 81 % porosity screen for  $Re_T = 1597$ . Time increases from (a) to (f).  $t^* = 0.0$  corresponds to the instance when the vortex ring is one diameter away from the wall. Reproduced from Adhikari and Lim [1]. **a**  $t^* = 1.49$ . **b**  $t^* = 1.67$ . **c**  $t^* = 1.89$ . **d**  $t^* = 2.07$ . **e**  $t^* = 2.28$ . **f**  $t^* = 4.23$

## 4 Effect of Porosity

Along the same line of investigation as Adhikari and Lim [1], Naaktgeboren et al. [41] conducted flow visualization studies and DPIV measurements to investigate the effect of screen porosity on a vortex ring as it interacts with a porous screen. Their flow visualization is limited to only one screen with an open-area ratio of about 58 %, wire diameter of 0.267 mm and pore aspect ratio of 1.57, whereas their DPIV measurements covered a wider range of open-area ratios from 0.44 to 0.79 and same nominal wire diameter of 0.7 mm and pore aspect ratio of one (square mesh). The test conditions were stroke-to-diameter ratio ( $L/D$ ) of 1.0 and 3.0 and nominal Reynolds numbers ( $Re_o = U_o D/\nu$ ), based on jet exit velocity ( $U_o$ ) and nozzle diameter ( $D$ ), of 3000 and 6000. Define in terms of initial circulation of vortex ring, the Reynolds number ( $Re_\Gamma = \Gamma/\nu$ ) for the case of  $Re_o = 3000$  is  $Re_\Gamma = 2500$  for  $L/D = 1$  and  $Re_\Gamma = 4800$  for  $L/D = 3$ . For the higher Reynolds number of  $Re_o = 6000$ , they are  $Re_\Gamma = 5700$  and 10000 for  $L/D = 1$  and 3, respectively. Unlike the porous screens used by Adhikari and Lim [1], which are specially fabricated so that the joints of the wires are fused together, the ones used by Naaktgeboren et al. [41] were purchased commercially with the wires woven similar that woven strings on a tennis racquet. It is not entirely clear whether the uneven surface affects the details of the interaction, but their flow visualization results appear to be broadly similar to that reported by Adhikari and Lim [1]. Quantitatively, their DPIV measurements show that the kinetic energy dissipation ( $\Delta E$ ) and reduction in impulse ( $\Delta I$ ) of a vortex ring after the interaction with a porous screen are dependent primarily on  $\phi$  with a slight decrease as  $L/D$  and/or  $Re$  is increased. They further found that the kinetic energy dissipation ( $\Delta E$ ) is strongly non-linear dependent in  $\phi$  whereas reduction in impulse ( $\Delta I$ ) is approximately linearly dependent in  $\phi$ .

## 5 Effect of Wire Diameter

Hrynyuk et al. [28] extended the studies of Adhikari and Lim [1] and Naaktgeboren et al. [41] to include the effect of wire diameters on a vortex ring during the interaction with porous surfaces. The study was conducted using flow visualization technique at Reynolds number ( $Re_m$ ) of the vortex ring (based on maximum ejection velocity ( $V_m$ ) and nozzle diameter ( $D_o$ )) of 2300–4200. The construct of the porous surfaces is similar to that used by Naaktgeboren et al. [41] and consists of woven stainless steel wires with square meshes. The open area of the porous surface or porosity was kept relatively constant while the wire diameter was varied from 0.018 to 0.267 cm. The detailed experimental parameters are depicted in Table 1. The visual results obtained by Hrynyuk et al. [28] are broadly similar to those reported by

**Table 1** Experimental parameters used by Hrynuk et al. [28]

Mesh (wire per cm)	Porosity (%)	Wire diameter (cm)
10.2	65	0.018 (fine)
4.3	64.5	0.046
2.4	62.7	0.089
2.0	63.2	0.104 (medium)
1.6	64	0.122
1.2	63.8	0.160
0.8	62.4	0.267 (Coarse)

Adhikari and Lim [1] and Naaktgeboren et al. [41] with a few exceptions which are wire diameter dependent. Based on the latter, they classified the vortex ring behavior into several regimes. For small wire diameter surface (i.e.  $d_w = 0.018$  cm), they found that the vortex ring that passed through the porous surface immediately reformed downstream. The transmitted ring was coherent and had a similar mean diameter as the primary vortex ring but lower circulation as is reflected in the slower propagation velocity (see Fig. 16). Their results also revealed the existence of secondary and tertiary vortex rings which orbited around the primary vortex ring before they merged to move away from the porous surface towards the vortex ring generator (see Fig. 16). With the wire diameter increased to  $d_w = 0.046$  cm, the vortex ring reformed further downstream of the surface (see Fig. 17), and as the wire diameter was increased further (i.e.  $d_w = 0.104$  cm), the transmitted vortex ring shows significant distortion downstream. It is not as coherent as in the case of small wire size and the ring also possess more fine-scale structures (see Fig. 17). For the coarse wire ( $d_w = 0.160$  cm), the transmitted ring is so highly distorted that it lost its coherent and accompanied by significantly more fine-scale structures. Generally, the larger mesh size or wire diameter requires a longer distance for the transmitted vortex ring to reform, and there are also more fine-scale scale structures on the transmitted ring. In all cases, secondary vortex ring was generated upstream of the porous surface but the extent of vortex ring rebound and speed of convection away from the porous surface decreased with larger wire size.

Hrynuk et al. [28] proposed a criterion to determine whether a primary vortex ring would immediately reform and/or breakup after passing through a porous surface. The criteria is based on an interaction Reynolds number ( $Re_i$ ), which they defined as

$$Re_i = \frac{U_c d_w}{\phi \nu}$$

where  $\phi$  is the screen porosity,  $U_c$  is pre-interaction propagation velocity of the vortex ring and  $d_w$  is the wire diameter. To test their hypothesis, two sets of experiments were conducted using vortex rings with initial Reynolds numbers of

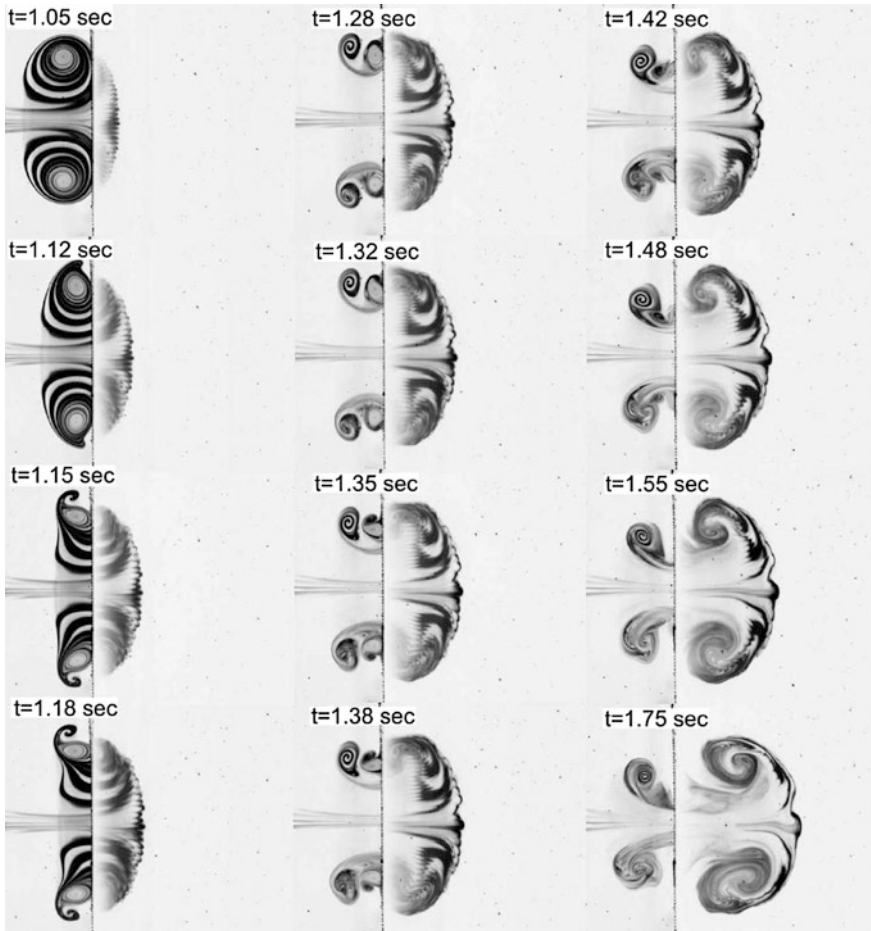
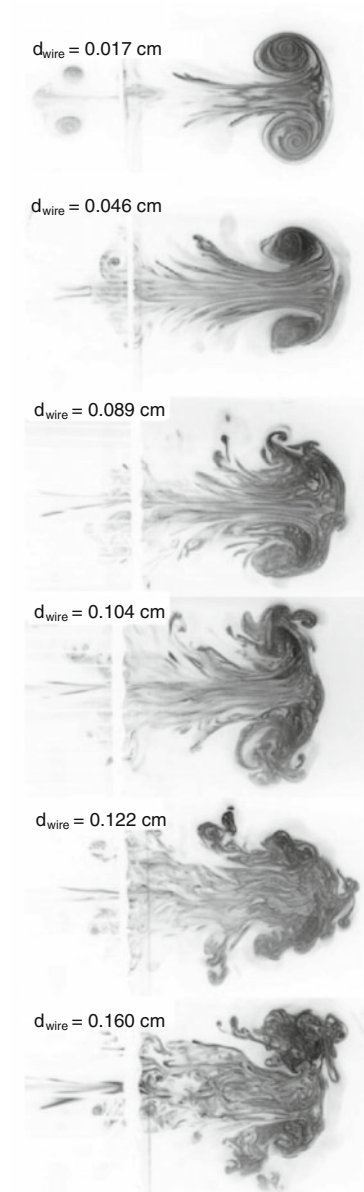


**Fig. 16** Detailed images of vortex ring interaction with fine screen. Reprinted with permission from Hrynuk et al. [28]. Copyright 2012, AIP Publishing LLC

( $Re_m$ ) of 2300 and 4200, and the results are presented in Fig. 18 for different interaction Reynolds number ( $Re_i$ ). Based on their findings, it appears that when  $Re_i < 63$ , the primary vortex ring, after passing through the porous surface, immediately reforms into coherent vortex ring. For  $63 < Re_i < 79$ , the reformation of the primary vortex ring is delayed downstream, which they attributed to the destabilization of the primary vortex ring caused by the generation of vortical sub-structures by the wires. For  $90 < Re_i < 164$ , the larger wire size causes the length-scale of vortical sub-structures to increase, resulting in partial reformation of the primary vortex ring. When  $Re_i > 203$ , the length-scale of the sub-structures is sufficiently large that they completely disrupt the vortex ring and the flow

**Fig. 17** LIF images showing vortex ring reformation as a function of wire diameter. The vortex rings are located at approximately  $3D_o$  downstream of the porous surface and  $Re_m = 4200$ . Reprinted with permission from Hrynuk et al. [28]. Copyright 2012, AIP Publishing LLC



eventually becomes turbulence. While the results of Hrynuk et al. [28] seems to suggest, at least qualitatively, the dependency of the state of the transmitted primary vortex ring on the interaction Reynolds number ( $Re_i$ ), further quantitative investigation is certainly needed to establish the exact relationship.



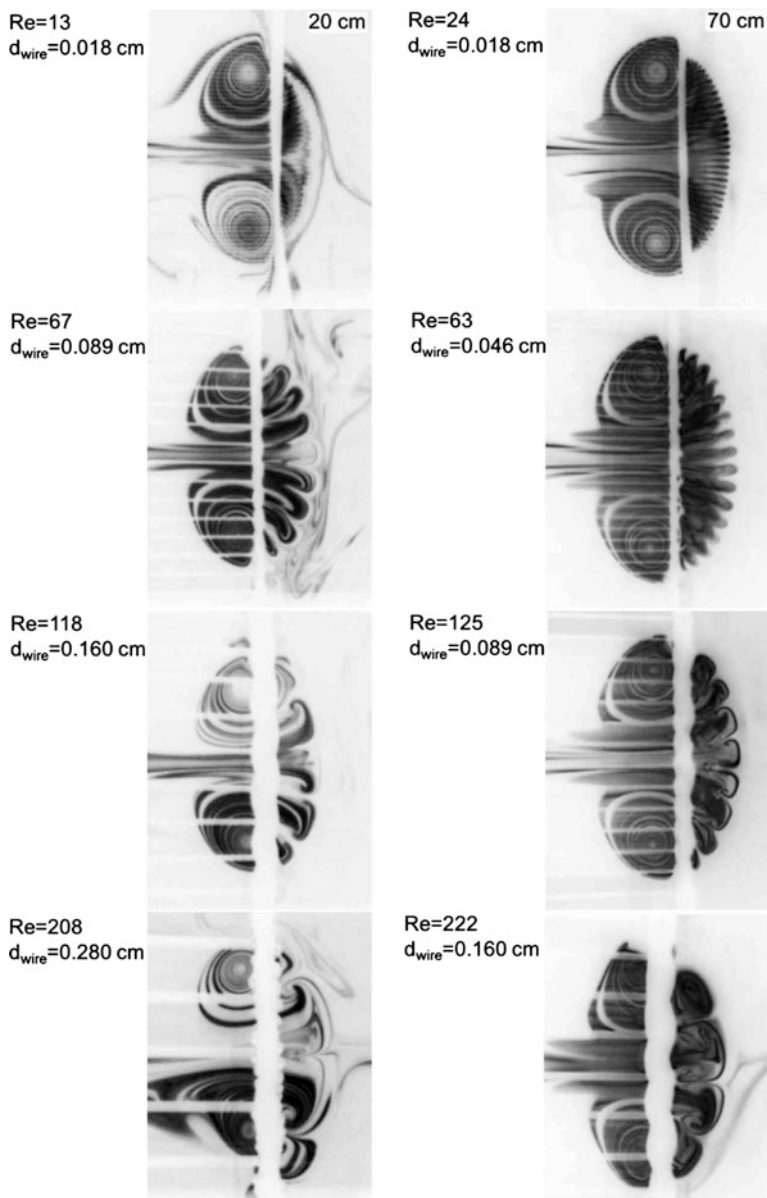


**Fig. 18** LIF images showing vortex ring reformation as a function of wire diameter. The vortex rings are located at approximately  $3D_0$  downstream of the porous surface and  $Re_m = 4200$ . Reprinted with permission from Hrynuik et al. [28]. Copyright 2012, AIP Publishing LLC

## 6 Summary

Although the above experimental studies have provided valuable insights into the dynamics of vortex ring/porous surface interaction, a shortcoming arising from these investigations is that porous screens of different construct were used. Hence, it is difficult to make meaningful comparison of the results obtained by different research groups. Furthermore, flow quantities such as evolution of core vorticity, changes in the kinetic energy and entropy across the screens are not easily measured experimentally. One fruitful mean of addressing these issues is to conduct numerical simulation of the interaction as it can provide far more detailed flow features and quantitative information than can be extracted from experiments. During the final editing this chapter, Cheng et al. [12] reported a numerical study on a vortex ring impacting a permeable wall over a wide range of parameters (i.e. open-area ratio, wire structure dimensions, wall thickness and Reynolds numbers) and addressed some of the above-mentioned issues.

## References

1. Adhikari, D., & Lim, T. T. (2009). The impact of a vortex ring on a porous screen. *Fluid Dynamics Research*, 41, 051404.
2. Akhmetov, D. G. (2009). *Vortex ring*. Berlin: Springer.
3. Akhmetov, D. G., Lugovtsov, B. A., & Tarasov, V. F. (1980). Extinguishing gas and oil well fires by means of vortex rings. *Combustion Explosion and Shock Waves*, 16(5), 490–494.
4. Ashurst, W. T., & Meiron, D. I. (1987). Numerical study of vortex reconnection. *Physical Review Letters*, 58, 1632–1635.
5. Auerbach, D. (1988). Some open questions on the flow of a circular vortex rings. *Fluid Dynamics Research*, 3, 209–213.
6. Barker, S., & Crow, S. (1977). The motion of two-dimensional vortex pairs in a ground effect. *Journal of Fluid Mechanics*, 82, 659–671.
7. Batchelor, G. K. (1974). *An introduction to fluid dynamics*. Cambridge: Cambridge University Press.
8. Boldes, U., & Ferreri, J. C. (1973). Behavior of vortex rings in the vicinity of a wall. *Physics of Fluids*, 16, 2005–2006.
9. Cerra, A. W., & Smith, C. R. (1983). Experimental observations of vortex ring interaction with the fluid adjacent to a surface. *Technical Report FM-4*. Bethlehem: Lehigh University.
10. Chahine, G. L., & Genoux, P. F. (1983). Collapse of a cavitating vortex ring. *Journal of Fluids Engineering Transaction of the ASME*, 105(4), 400–405.
11. Chatelain, P., Kivotides, D., & Leonard, A. (2003). Reconnection of colliding vortex rings. *Physical Review Letters*, 90(5), 054501.
12. Cheng, M., Lou, J., & Lim, T. T. (2014). A numerical study of a vortex ring impacting a permeable wall. *Physics of Fluids*, 26, 103602.
13. Cheng, M., Lou, J., & Luo, L. S. (2010). Numerical study of a vortex ring impacting a flat wall. *Journal of Fluid Mechanics*, 660, 430–455.
14. Chu, C. C., & Falco, R. E. (1998). Vortex ring and viscous wall layer interaction model and turbulence production process near wall. *Experiments in Fluids*, 6, 305–325.
15. Chu, C. C., Wang, C. T., & Chang, C. C. (1995). A vortex ring impinging on a solid plane surface-vortex structure and surface force. *Physics of Fluids A*, 7(60), 1391–1401.

16. Dabiri, J. O. (2009). Optimal vortex formation as a unifying principle in biological propulsion. *Annual Review of Fluid Mechanics*, 42, 17–33.
17. Dabiri, J. O., Colin, S. P., & Costello, J. H. (2006). Fast-swimming hydromedusae exploit velar kinematics to form an optimal vortex wake. *Journal of Experimental Biology*, 209, 2025–2033.
18. Dhanak, M. R., & Bernardinis, D. E. B. (1981). The evolution of an elliptic vortex ring. *Journal of Fluid Mechanics*, 109, 189–216.
19. Didden, N. (1979). On the formation of vortex rings: Rolling-up and production of circulation. *Journal of Applied Mechanics Physics (ZAMP)*, 30, 101–116.
20. Doligalski, T. L., Smith, C. R., & Walker, J. D. A. (1994). Vortex interactions with walls. *Annual Review of Fluid Mechanics*, 26, 573–616.
21. Fabris, D., Liepmann, D., & Marcus, D. (1996). Quantitative experimental and numerical investigation of a vortex ring impinging on a wall. *Physics of Fluids*, 8, 2640–2649.
22. Fohl, T. (1967). Optimization of flow for forcing stack wastes to high altitudes. *Journal of Air Pollution Control Association*, 17, 730–733.
23. Fukumoto, Y., & Moffatt, H. K. (2008). Kinematic variational principle for motion of vortex ring. *Physics D*, 237, 2210–2217.
24. Gan, L., & Nickels, T. B. (2010). An experimental study of turbulent vortex rings during their early development. *Journal of Fluid Mechanics*, 64, 467–496.
25. Gharib, M., Rambod, E., & Shariff, K. (1998). A universal time scale for vortex ring formation. *Journal of Fluid Mechanics*, 360, 121–140.
26. Glezer, A., & Coles, D. (1990). An experimental study of a turbulent vortex ring. *Journal of Fluid Mechanics*, 211, 243–283.
27. Harvey, J., & Perry, F. (1971). Flowfield Produced by Trailing Vortices in the Vicinity of the Ground. *AIAA Journal*, 9(8), 1659–1660.
28. Hrynuk, J. T., Luipen, J. V., & Bohl, D. (2012). Flow visualization of a vortex ring interaction with porous surfaces. *Physics of Fluids*, 24, 037103.
29. Kambe, T., & Takao, T. (1971). Motion of distorted vortex rings. *Journal of the Physical Society of Japan*, 31, 591–599.
30. Kida, S., & Takaoka, M. (1994). Vortex reconnection. *Annual Review of Fluid Mechanics*, 26, 169–189.
31. Kida, S., Takaoka, M., & Hussain, F. (1991). Collision of two vortex rings. *Journal of Fluid Mechanics*, 230, 583–646.
32. Lim, T. T. (1997). On the role of Kelvin-Helmholtz-like instability in the formation of turbulent vortex rings. *Fluid Dynamics Research*, 21(1), 47–56.
33. Lim, T. T., & Nickels, T. B. (1995). Vortex rings. In S. I. Green (Ed.), *Fluid Vortices* (pp. 95–153). Netherlands: Springer.
34. Lim, T. T., Nickels, T. B., & Chong, M. S. (1991). A note on the cause of rebound in the head-on collision of a vortex ring with a wall. *Experiments in Fluids*, 12, 41–48.
35. Lundgren, T. S., & Mansour, N. N. (1991). Vortex ring bubbles. *Journal of Fluid Mechanics*, 224, 177–196.
36. Magarvey, R. H., & MacLachy, C. S. (1964). The disintegration of vortex rings. *Canadian Journal of Physics*, 42, 678–689.
37. Marten, K., Shariff, K., Psarakos, S., & White, D. J. (1996). Ring bubbles of dolphins. *Scientific American*, 275, 83.
38. Maxworthy, T. (1972). The structure and stability of vortex rings. *Journal of Fluid Mechanics*, 51, 15–32.
39. Maxworthy, T. (1974). Turbulent vortex rings. *Journal of Fluid Mechanics*, 64, 227–240.
40. Melander, M., & Hussain, F. (1989). Cross-linking of two antiparallel vortex tubes. *Physics of Fluids A*, 1, 633–636.
41. Naaktgeboren, C., Krueger, P. S., & Lage, J. L. (2012). Interaction of a laminar vortex ring with a thin permeable screen. *Journal of Fluid Mechanics*, 707, 260–286.
42. Orlandi, P., & Verzicco, R. (1993). Vortex ring impinging on a wall: Axisymmetric and three-dimensional simulations. *Journal of Fluid Mechanics*, 256, 615–646.

43. Reynolds, O. (1876). On the resistance encountered by vortex rings and relation between the vortex rings and the streamlines of a disk. *Nature*, 14, 477–479.
44. Saffman, P. G. (1970). The velocity of viscous vortex rings. *Studies in Applied Mathematics*, 49, 71–380.
45. Saffman, P. G. (1978). The number of waves on unstable vortex rings. *Journal of Fluid Mechanics*, 84, 625–639.
46. Saffman, P. G. (1990). A model of vortex reconnection. *Journal of Fluid Mechanics*, 212, 395–402.
47. Saffman, P. G. (1992). *Vortex dynamics*. Cambridge: Cambridge University Press.
48. Shariff, K., & Leonard, A. (1992). Vortex Rings. *Annual Review of Fluid Mechanics*, 24, 235–279.
49. Thomson, W., & Kelvin, L. (1867). On vortex atoms. *Philosophical Magazine*, 34, 15–24.
50. Tsai, C. Y., & Widnall, S. E. (1976). The stability of short waves on a straight vortex filament in a weak externally imposed strain field. *Journal of Fluid Mechanics*, 73, 721–733.
51. Turner, J. S. (1960). Intermittent release of smoke from chimneys. *Journal of Mechanical Engineering Science*, 2, 97–100.
52. Walker, J. D. A., Smith, C. R., Cerra, A. W., & Doligalski, T. L. (1987). The impact of a vortex ring on a wall. *Journal of Fluid Mechanics*, 181, 99–140.
53. Widnall, S. E., Bliss, D. B., & Tsai, C. Y. (1974). The instability of short waves on a vortex ring. *Journal of Fluid Mechanics*, 66, 35–47.
54. Widnall, S. E., & Sullivan, J. P. (1973). On the stability of vortex rings”. *Proceedings of the Royal Society of London A*, 332, 335–353.
55. Widnall, S. E., & Tsai, C. Y. (1977). The instability of a thin vortex ring of constant vorticity. *Philosophical Transactions of the Royal Society of London A*, 287, 273–305.
56. Yamada, H., Kohsaka, T., & Yamabe, H. (1982). Flowfield produced by a vortex ring near a plane wall. *Journal of the Physical Society of Japan*, 51, 1663–1670.

Vortex Rings and Jets

Recent Developments in Near-Field Dynamics

New, D.T.H.; Yu, S. (Eds.)

2015, IX, 235 p. 147 illus., 81 illus. in color., Hardcover

ISBN: 978-981-287-395-8